ROYAL SOCIETY OF CHEMISTRY

Check for updates

Persistent triboelectrification-induced electroluminescence for self-powered all-optical wireless user identification and multi-mode anti-counterfeiting†

Li Su,[a] Zihan Wang,[d] Chengyue Lu,[d] Wenbo Ding,[d] Yong Zhao [ID][a] and Yunlong Zi [ID] *[bc]

Persistent triboelectrification-induced electroluminescence (TIEL) is highly desirable to break the constraints in the transient-emitting behavior of existing TIEL technologies as it addresses the hindrance caused by incomplete information in optical communication. In this work, a novel self-powered persistent TIEL material (SP-PTM) has been created for the first time, by incorporating the long-afterglow phosphors $SrAl_2O_4:Eu^{2+}$, Dy^{3+} (SAOED) in the material design. It was found that the blue-green transient TIEL derived from ZnS:Cu, Al serves as a reliable excitation source to trigger the persistent photoluminescence (PL) of SAOED. Notably, the aligned dipole moment formed along the vertical direction in the bottom ferro-electric ceramics layer acts as an "optical antenna" to promote variation in the electric field of the upper luminescent layer. Accordingly, the SP-PTM exhibits intense and persistent TIEL for about 10 s in the absence of a continuous power supply. Due to such unique TIEL afterglow behavior, the SP-PTM is applicable in many fields, such as user identification and multi-mode anti-counterfeiting. The SP-PTM proposed in this work not only represents a breakthrough in TIEL materials due to its recording capability and versatile responsivity but also contributes a new strategy to the development of high-performance mechanical-light energy-conversion systems, which may inspire various functional applications.

New concepts

Due to various unique advantages over conventional mechanolumines-cence (ML), such as non-destructive nature, high stress responsivity, and low stress-threshold value, triboelectrification-induced electroluminescence (TIEL) has shown a massive potential in assisting the development of intelligent optical materials. However, it remains challenging to break the limitations of the transient emission behavior of the existing TIEL technologies. In this study, a novel self-powered persistent TIEL material (SP-PTM) is produced by incorporating the long-afterglow phosphors $SrAl_2O_4:Eu^{2+}$, Dy^{3+} (SAOED) into the design of the TIEL material. Through the aligned dipole moment generated vertically in the bottom ceramics layer, which acts as an "optical antenna", the variation of the electric field in the upper luminescent layer is promoted. Meanwhile, the SP-PTM exhibits intense and persistent TIEL for about 10 s in the absence of a continuous power supply. In line with a novel methodology for TIEL afterglow, this SP-PTM with a designed architecture demonstrates advantages, such as low cost, ease of manufacturing, practicability, and a huge potential for large-scale applications. It may present great opportunities for the development of high-performance mechanical-light energy-conversion systems with recording capability and versatile responsivity, thus expanding the scope of their applications.

1. Introduction

Mechanoluminescence (ML) refers to a smart light-emitting characteristic that can convert mechanical energy directly to luminescence and has led to the rapid progress of widespread applications, including passive self-powered illumination and displays,[1,2] real-time vision sensors,[3–5] and wearable devices.[6,7] In particular, triboelectrification-induced electroluminescence (TIEL) is classified as a novel type of ML, which is based on the coupling effect of triboelectrification and electroluminescence (EL) with an essential difference from conventional ML generally caused by the piezoelectric effect.[8–12] It has been found that this TIEL phenomenon is characterized by the non-destructive property, high-stress responsivity, and a low stress-threshold value (far exceeding that of conventional ML), which make it a promising candidate for developing intelligent optical systems.[13–17] Until now, most of the existing ML or TIEL materials are intrinsically

[a] *Hebei Key Laboratory of Micro-Nano Precision Optical Sensing and Measurement Technology, School of Control Engineering, Northeastern University at Qinhuangdao, Qinhuangdao, Hebei 066004, China*

[b] *Thrust of Sustainable Energy and Environment, The Hong Kong University of Science and Technology (Guangzhou), Nansha, Guangdong 511400, China. E-mail: ylzi@ust.hk*

[c] *HKUST Shenzhen-Hong Kong Collaborative Innovation Research Institute, Futian, Shenzhen, Guangdong 518048, China*

[d] *Tsinghua-Berkeley Shenzhen Institute, Shenzhen International Graduate School, Tsinghua University, Shenzhen 518055, China*

† Electronic supplementary information (ESI) available. See DOI: https://doi.org/10.1039/d3mh00172e

capable of exhibiting instantaneous luminescence with responsiveness in the sub-millisecond (ms) level, which provides an effective solution for real-time visualized sensing.[18–20] However, despite these achievements, complex equipment is still required for the capture of transient-light signals with complete information. Hence, it is reasonable to extend the duration of luminescence and achieve persistent TIEL afterglow, which enables delayed display and visualization. Undoubtedly, this would lead to TIEL-enabled communication with complete information, high convenience, and practicability.

Recently, novel ML materials obtained by reshuffling the trap occupations of the charge carriers have been demonstrated, thus leading to persistent ML read-outs over a longer duration to address the drawbacks caused by transient ML. However, the reported persistent ML still requires pre-irradiation treatment to pre-charge energy in most cases, and it diminishes after a sufficient number of carriers in the traps are released, which increases the difficulty of its application.[21,22] In our previous study, we demonstrated the wide-spectrum manipulation of TIEL, involving the use of the long-afterglow phosphor to absorb the green TIEL from the ZnS:Cu before its conversion to blue and red photoluminescence (PL) through photo-induced charge carrier excitation.[23,24] Meanwhile, several studies have revealed such phenomena in various mechanical-light energy conversion systems.[5,6,25,26] However, the limited TIEL intensity usually gives rise to inconspicuous afterglow, which is insufficient to obtain persistent TIEL in practice. Inspired by these works, we hypothesize that persistent TIEL may be accomplished through materials with stronger excitation and an appropriate structural design. On this basis, the solution to achieving the urgent TIEL afterglow can be found, and the scope of TIEL-related practical applications can be further expanded.

Moreover, with the recent advancements in TIEL technologies, it is evident that the regulation of the amplitude value and time interval of dynamic motion can contribute to variations in the electric field, which provides two effective approaches to achieve considerably high TIEL intensity and an insight into the design of TIEL materials.[15,18,27,28] However, the reported TIELs are generally radiated in all directions in free space, which severely restricts the collection and detection of photons. In terms of developing design theories for TIEL materials toward outstanding optical performance, it remains a tough challenge to impose control on the radiation characteristics of TIEL. Nevertheless, a few works have focused on these issues.

In this work, for the first time, a novel self-powered persistent TIEL material (SP-PTM) was obtained by incorporating the long afterglow phosphors $SrAl_2O_4:Eu^{2+}, Dy^{3+}$ (SAOED) in the design. Stemming from the persistent photoluminescence (PL) of SAOED, the afterglow was excited by the blue-green TIEL radiation from ZnS:Cu, Al. More importantly, the aligned dipole moment formed along the vertical direction in the bottom ferroelectric ceramic layer could be used to regulate the direction of the electric field and enhance the variation in the electric field of the upper luminescent layer. Therefore, the SP-PTM exhibited intense and persistent TIEL afterglow for 10 s in the absence of a continuous power supply. Furthermore, the SP-PTM was employed in all-optical wireless user identification and multi-mode anti-counterfeiting, showing its potential applications in mechanical monitoring, human–machine interface, blockchain, and other related fields. This work contributes a facile approach to obtaining persistent TIEL with a designed architecture and various advanced features, thus presenting new opportunities for developing high-performance mechanical-light energy conversion systems and functional TIEL-related applications.

2. Results and discussion

The fabrication of the SP-PTM followed the typical structural design of a TIEL material, as illustrated in Fig. 1a. The sequentially constructed composite consisted of four layers: a flexible substrate, an enhancement layer made of ferroelectric PZT ceramics, a luminescent layer comprising of a polydimethylsiloxane (PDMS) matrix embedded with the EL phosphor ZnS:Cu, Al and the long-persistent PL phosphor SAOED, as well as an electrification layer made of ethylene propylene (FEP). The fabrication process is detailed in the Experimental Section (ESI†). The scanning electron microscopy (SEM) images of the phosphors and ferroelectric ceramics are shown in the right section. The X-ray diffraction pattern (XRD) and the energy-dispersive spectroscopy (EDS) results in Fig. S1 (ESI†) reveal the composition of the above phosphors. Fig. 1b shows the afterglow mapping of the SP-PTM and the comparison of the decay curves of SP-PTM and pristine TIEL. Notably, SP-PTM was effective in extending the transition time to 10 s without any pre-irradiation requirement. Particularly, SAOED encapsulated with different fluorescent agents displayed various afterglow colors (blue, green, and orange) under sliding stimulation,[26] as revealed in Fig. S2 (ESI†). Due to this unique TIEL afterglow behavior, the SP-PTM is widely applicable in various advanced settings, such as user identification and multi-mode anti-counterfeiting, showing its application potential in mechanical monitoring, human–machine interface, blockchain, and other related fields, as exhibited in Fig. 1c. Fig. 1d presents the comparison of the emission spectra of pristine TIEL, SP-PTM, and PL of SAOED (orange light), which were obtained by using the constructed test platform shown in Fig. S3 (ESI†). As confirmed by the obtained emission spectra, the SP-PTM showed intense luminescence, which was almost identical to the PL spectra of SAOED. This suggests that the persistent TIEL of SP-PTM involves the same emission process of electron–hole recombination within the luminescent Eu^{2+} centers as in SAOED. Moreover, the intensity of the SP-PTM was restored rapidly under sliding stimuli, showing no degradation under cycle tests, indicating its high resilience and excellent recoverability (Fig. 1e). In order to demonstrate the underlying mechanism of the TIEL afterglow, a detailed working mechanism of SP-PTM involving the conjunction effect of tribo-electrification, EL and PL is illustrated in Fig. 1f. In the initial state (I), when the external object contacts the electrification layer, the same amount of negative and positive charges are generated on the surfaces of the electrification layer and the external object. Immediately after the external object slides out of the SP-PTM, a
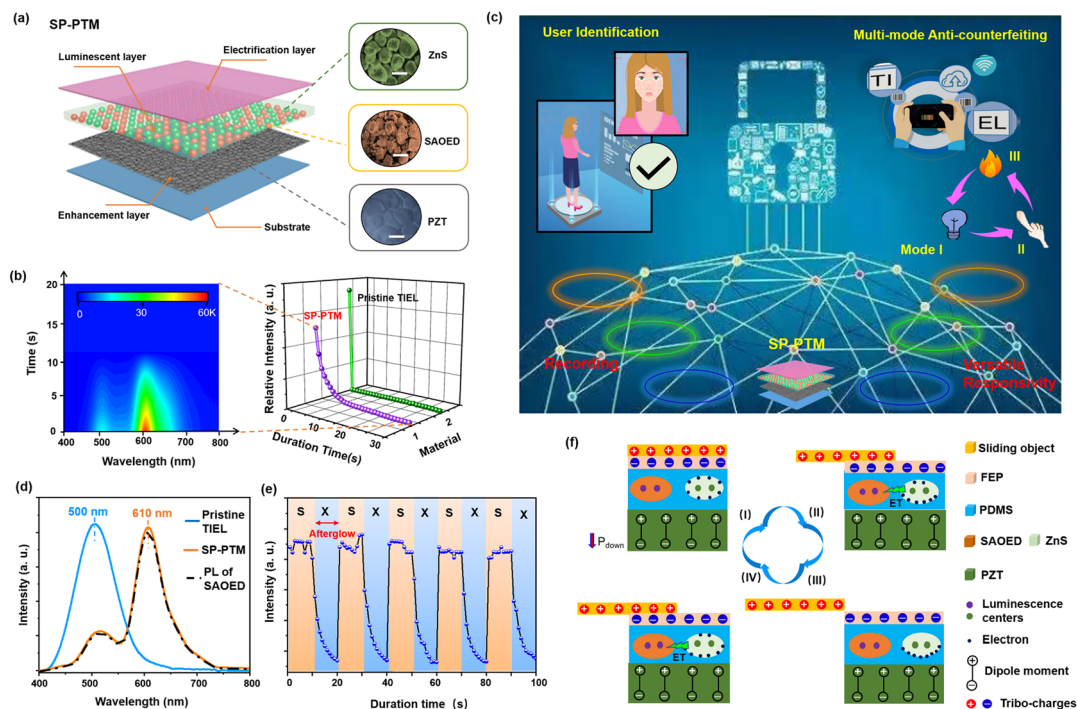
Fig. 1 The design of the SP-PTM and its working mechanism. (a) Schematic of the SP-PTM. Right section: The SEM images of the phosphors and ferroelectric ceramics, scale bar: 30 μm. (b) The afterglow mapping of the SP-PTM. Right section: a comparison of the decay curves of the SP-PTM and the well-studied pristine TIEL. (c) The prospective application of the SP-PTM in all-optical wireless user identification and multi-mode anti-counterfeiting. (d) Comparison of the emission spectra of pristine TIEL and SP-PTM developed in this work, as well as the PL spectra of SAOED. (e) The rapid recovery of SP-PTM under sliding stimuli without any pre-irradiation. The symbols "S" and "X" along the time axis represent sliding and stoppage of sliding, respectively. (f) Schematic of the working mechanism of SP-PTM involving four typical working states.

rapidly varying electric field is created in the luminescent layer. Excited by this varying electric field, the electrons generated in the lattice by impact ionization migrate to the bottom of the ZnS phosphors. The moving electrons are excited by high energy in the luminescence centers of the ZnS:Cu, Al phosphor in the form of impact excitation, which leads to blue-green emission through radiative recombination. In this way, the photoionized electrons in the SAOED phosphors are released to the excited state by TIEL radiation through energy transfer (ET) to achieve persistent PL emission. When the external object slides out of the SP-PTM completely (state III), all electrons are concentrated at the bottom of the ZnS:Cu, Al phosphor, as driven by the electric field. Currently, no emission occurs due to the interaction between the moving electrons and the luminescence centers. When the external object slides backward, the electrons at the bottom of the ZnS:Cu, Al phosphor move back up and excite the luminescence centers to generate EL, thus leading to the recurrence of persistent PL emission (state IV). In this case, the alternating-current (AC)-like dynamic varying electric field induced by triboelectrification consequently produces the EL radiation of the ZnS:Cu, Al phosphor in the luminescent layer and then excites the adjacent persistent PL phosphor SAOED through an ET process, along with phosphorescence emission.

Furthermore, in order to obtain a full understanding of the above working mechanism, the software package COMSOL Multiphysics was applied to simulate the electric field distribution in pristine TIEL and SP-PTM at the four working states I to

IV depicted in Fig. 1f. Two-dimensional (2D) models were constructed under the settings discussed in Fig. S4 and Note S1 (ESI†) with comparable dimensions to those of actual materials, along with identical absolute charge density. The black arrows indicate the direction of the electric field. It was found that the electric field lines in pristine TIEL diverged away from the positively charged sliding object with transverse divergence, indicating a low electric field in the vertical direction, as shown in Fig. 2a. Fig. 2b and c present the cross-sectional view of the electric field distribution of SP-PTM in one complete working cycle, in which P_{down} and P_{up} represent the pointing directions of the dipole moment in the PZT ceramic layer, respectively. Due to the pre-polarization of the ceramic layer, the aligned dipole moment is produced along the vertical direction owing to its corresponding large remanent polarization (Fig. S5, ESI†). The induced aligned dipole moment draws the electric field lines perpendicular to the ceramic layer, due to which the distribution of the electric field within the motion of the sliding object is confined vertically with reduced divergence in the lateral direction (Fig. S6, ESI†). In this regard, the amplitude of the electric field at the center point "P" of the luminescent layer in the four typical working states was extracted by COMSOL simulation, as revealed in Fig. 2d. It thus shows that the vertical electric field variation (ΔE) at the center point "P" of the pristine TIEL was only 0.65 MV m^{-1} in one working cycle compared to 1.38 MV m^{-1} in the SP-PTM, confirming the significant improvement in electric field variation due to the ceramic layer, which effectively promotes
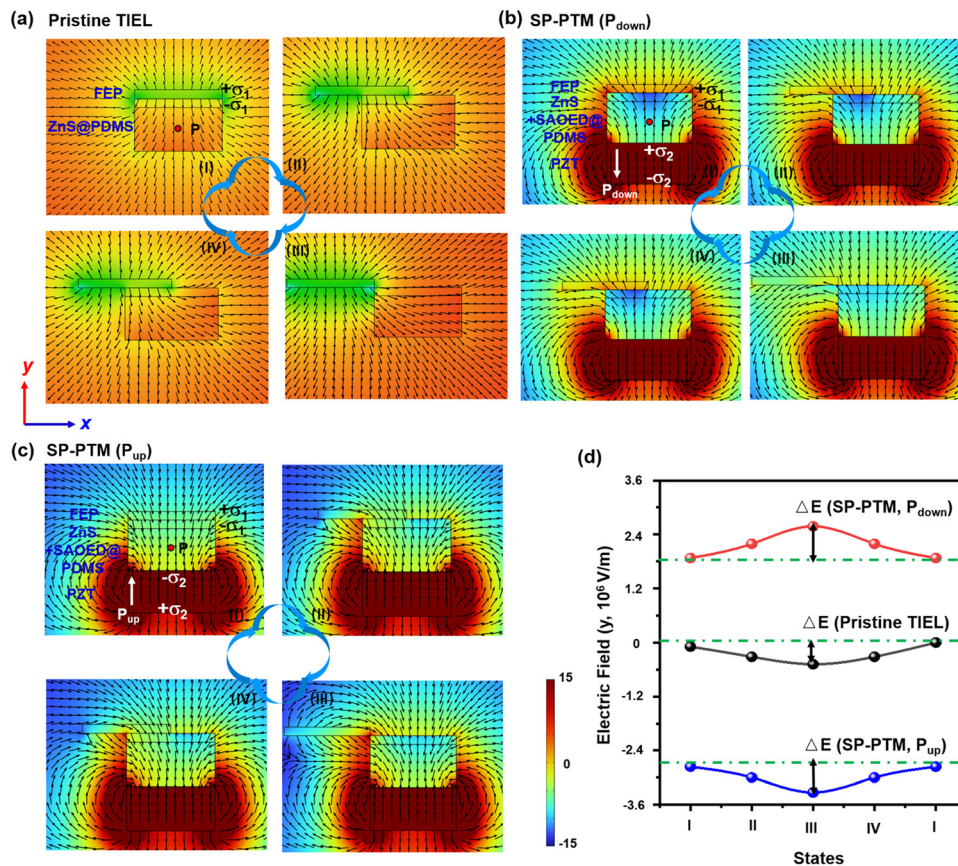
Fig. 2 The COMSOL simulation. The 2D models of the electric field distribution across the cross-section of (a) pristine TIEL, (b) SP-PTM (P_{down}), and (c) SP-PTM (P_{up}) in the four typical working states, as constructed using the COMSOL software. (d) The extracted electric field value at the center point "P" of the luminescent layer in the four typical working states of pristine TIEL and SP-PTM, respectively.

the TIEL intensity. As a result, the stronger EL of ZnS:Cu, Al excites the persistent PL phosphor SAOED, thus leading to persistent TIEL along the sliding trajectory. These simulation results not only demonstrate the design concept of SP-PTM but also further confirm the working mechanism of the SP-PTM proposed in Fig. 1f.

Apparently, the duration of the TIEL afterglow was proportional to its intensity. To further optimize the optical performance, the factors influencing the TIEL intensity of SP-PTM were explored by controlling several variables. The SAOED content in the luminescent layer determined the TIEL intensity, as shown in Fig. 3a. The intensity at 610 nm reached an optimal level at the 30% mass ratio of the SAOED phosphor (Fig. 3b) in the whole luminescent layer, and the conversion efficiency is calculated in Fig. S7 (ESI†). Meanwhile, the corresponding Commission Internationale de l'Eclairage (CIE) coordinates (x, y) shifted from transient green TIEL (0.18, 0.46) to persistent orange PL (0.54, 0.37) (Fig. 3c). However, excessive SAOED phosphor content reduced the light emission due to the quenching effect at high concentrations. The excitation and absorption spectra of SAOED can be used to explain this conversion, as shown in Fig. 3d. The afterglow of SAOED can be produced by trap-filling and detrapping after irradiation with different wavelengths. In brief, a forward electron transfer

from Eu^{2+} to Dy^{3+} is induced by UV or blue light irradiation, while the reverse electron transfer is achieved by illuminating the phosphors with green to red light.[29] The excitation band (400–500 nm) of SAOED and absorption band (500–600 nm) of the filled traps were found to almost overlap with the green TIEL emission of ZnS (400–600 nm), with a high conversion efficiency of 85.3% between these two phosphors. Additionally, an in-depth investigation was conducted into the impact of PZT polarization, sliding materials, pressure at the contact surface, and motion frequency on the TIEL intensity, as shown in Fig. 3e and Fig. S8 (ESI†). Firstly, with the ceramic enhancement layer applied at the bottom of the luminescent layer, the intensity of SP-PTM improved by two orders of magnitude compared with that without the ceramic enhancement layer, which is attributed to the enhanced electric field of the luminescent layer in the vertical direction (Movie S1, ESI†). This is consistent with the results of COMSOL simulation (Fig. 2b, c, and Fig. S3, ESI†). Secondly, the sliding material is considered a major contributor to achieving maximum contact electrification. The significant difference in triboelectric polarity between the sliding material and the electrification layer (FEP) leads to the high tribo-charge density, as well as the high TIEL intensity. Thirdly, the TIEL intensity is largely dependent on the stress arising at the contact surface. The intensity increased almost linearly with
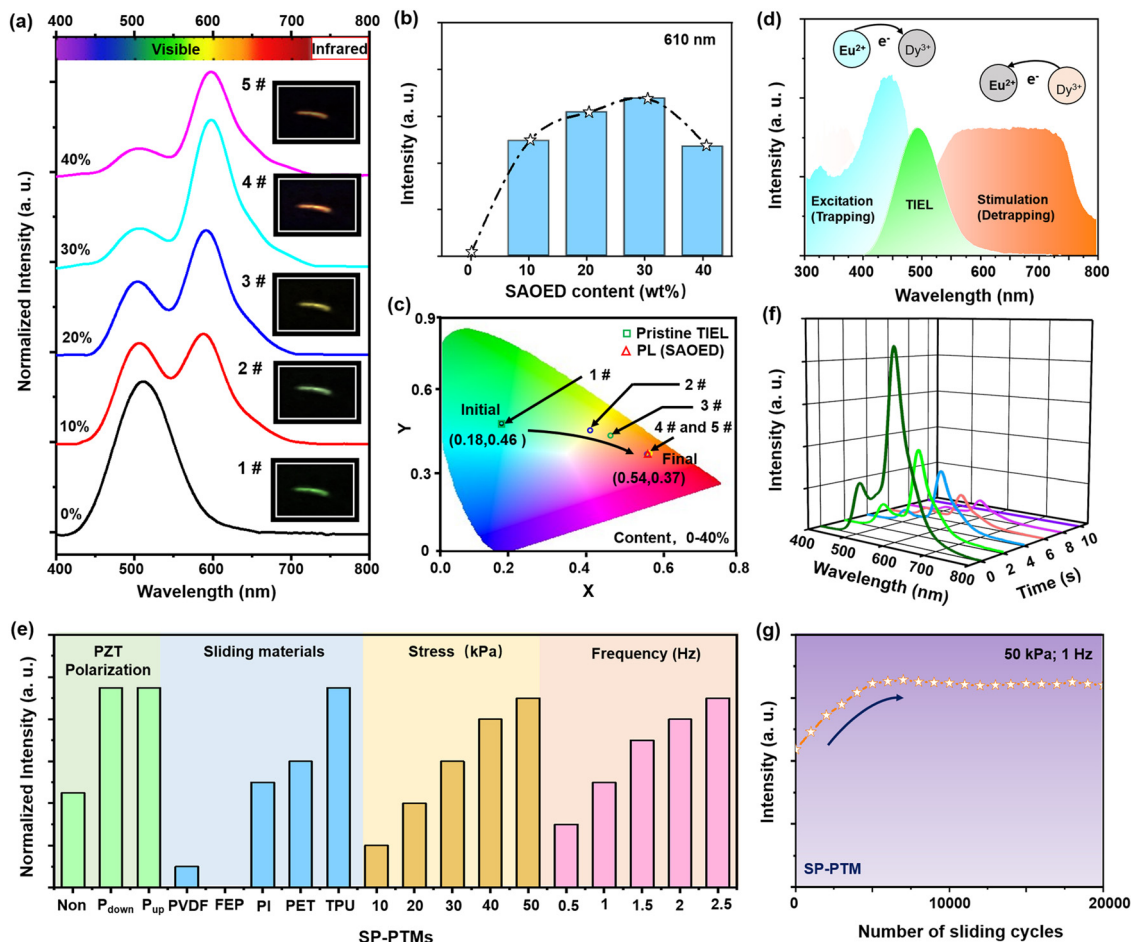
Fig. 3 The optical performance of SP-PTM. (a) The TIEL spectra, (b) TIEL intensity at 610 nm and (c) the corresponding CIE coordinates (*x*, *y*) with different SAOED contents in the luminescent layer. The inset of (a): The corresponding optical photographs of the SP-PTMs. (d) The excitation spectrum of SAOED (blue curve) and the absorption spectrum of the filled traps (orange curve) together with the TIEL emission spectrum. (e) The impact of the polarization of ferroelectric PZT, different sliding materials, different applied stress from 10 to 50 kPa, and frequency range from 0.5 to 2.5 Hz on the TIEL intensity of the SP-PTMs. (f) The test of the TIEL duration of SP-PTM by using the optimized parameters. (g) The stability and repeatability tests of SP-PTM.

stress, and the emission tended to be saturated beyond 40 kPa owing to the maximum tribo-charge density. Finally, the TIEL intensity showed a substantial improvement as the motion frequency increased sharply from 0.5 to 2.5 Hz, which is possibly attributed to the rise in electrons in the ZnS:Cu, Al phosphors within a unit time interval to effectively activate the luminescent centers. By using the optimized parameters (with the polarized enhancement layer, the sliding material TPU, 50 kPa, and 1 Hz), the TIEL duration of the SP-PTM was tested, as shown in Fig. 3f. The TIEL afterglow lasted for about 10 s without any pre-irradiation. Furthermore, the repeatability and stability of the TIEL performance of SP-PTM were also evaluated after 20 000 cycles (Fig. 3g). Unlike the stable pristine TIEL emission (Fig. S9, ESI†), the intensity of SP-PTM increased initially and then stabilized after a few cycles. The result can be attributed to the complement and recombination of the carriers in the trap energy level of SAOED, which tends to get balanced over time, thus leading to a relatively stable intensity.

Furthermore, the persistent afterglow performance obtained in this work and other recent reports were compared, as shown in Fig. 4a and Fig. S10 (ESI†). In most previous works, ML and TIEL exhibit instantaneous light-emitting behavior, and the illumination disappears immediately after the withdrawal of mechanical stimuli. For the SP-PTM with an enhancement layer proposed in this study, the duration time of SP-PTM was extended to 10 s (Movie S2, ESI†), which is comparable to that of the self-charging persistent ML reported in the literature.[30–32] The only work reporting a longer TIEL duration of 20 s required the pre-irradiation treatment.[22] It is worth noting that after pre-irradiation with ultraviolet (UV) light, the duration of SP-PTM could be further extended to about 20 s in this work as well. Evidently, the afterglow intensity of SAOED is proportional to the number of filled traps. Therefore, a further investigation was conducted on the effect of the charge carrier transitions and the energy transfer pathways in the traps of SP-PTM. To ensure the storage of a large number of electrons in the traps, the thermoluminescence (TL) spectra of ZnS:Cu, Al and SAOED were measured after irradiation under a 365 nm UV light. Different from the TL peak of ZnS:Cu, Al located at 256 K, SAOED exhibited a long-lasting afterglow behavior, which is
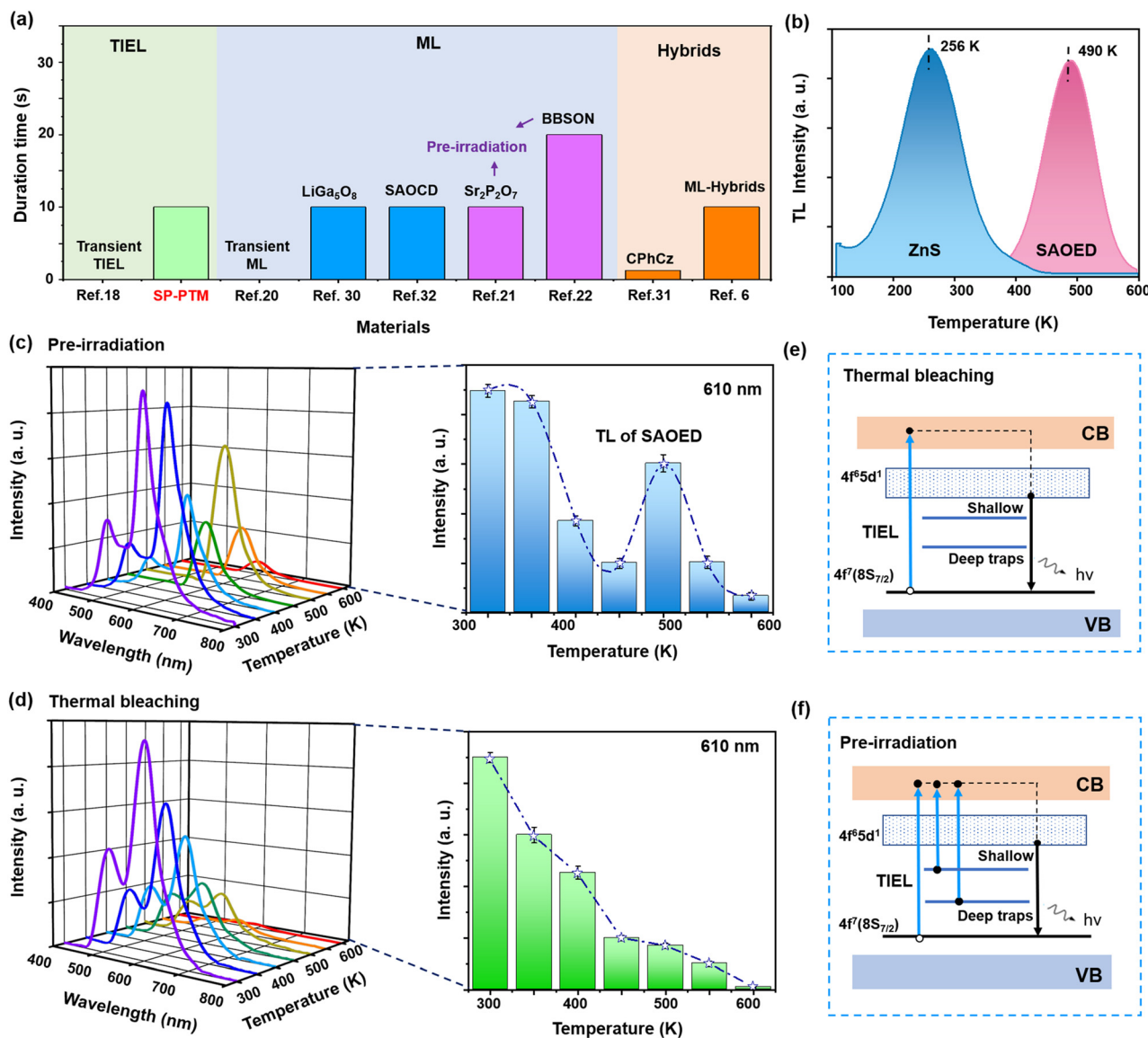
Fig. 4 The charge carrier transitions and energy transfer pathways in SP-PTM. (a) Comparison of the duration times of SP-PTM and persistent ML in recent literature. (b) The TL glow curves of ZnS:Cu, Al and SAOED after irradiation under a 365 nm UV light at RT for 5 min. The emission spectra and intensity of SP-PTM at 610 nm after (c) UV irradiation and (d) thermal bleaching. The energy-level schematic for the persistent TIEL processes in SP-PTM under (e) thermal bleaching and (f) pre-irradiation.

attributed to the trap state at a deeper position (490 K). The stored energy is further released after heat treatment and is completely removed when the temperature reaches 450 K in ZnS:Cu, Al and at 600 K in SAOED (Fig. 4b), respectively, which is consistent with the previous reports.[29,33] Moreover, the TIEL spectra of the SP-PTM after UV irradiation were measured after heat treatment at different temperatures, as shown in Fig. 4c. In the low-temperature region from 300 to 450 K, the emission intensity declined gradually. Despite this, a higher intensity was reached when the temperature was further raised from 450 K to 600 K, due to the release of the stored electrons. The corresponding intensity was consistent with the trend of changes in the TL curve, which supports the inference that the TIEL afterglow results from the release of trapped energy.

Notably, the traps are cleaned in this step by the high-temperature procedure, which is known as "thermal bleaching" (Fig. S11, ESI†). Subsequently, the SP-PTM with cleaned traps is cooled down to room temperature (RT) in darkness, and the TL glow of SAOED is eliminated prior to the next temperature-dependent TIEL test. Desirably, the remaining TL signals of SAOED were produced in the high-temperature region beyond 450 K (Fig. 4d). The results show that the involvement of TIEL radiation can enable the self-energy-charging of SAOED instead of being only dependent on the pre-stored energy in the traps. Therefore, based on the afore-mentioned experiment, the energy level diagram of SAOED was further established to fully explain the mechanism of the SP-PTM. As for the SP-PTM, after thermal bleaching, there are few

electrons on the trap levels. TIEL can be used to directly induce the transition of Eu^{2+} from the ground state to the conduction band (CB), showing an ordinary persistent TIEL emission (Fig. 4e). Besides, after the pre-irradiation of the SP-PTM under a UV light, a large number of electrons are captured and stored in the traps. Upon TIEL radiation, these electrons can be released again to CB and then supplied for the transition of Eu^{2+} to extend the persistent TIEL (Fig. 4f). Therefore, the observed persistent TIEL of SP-PTM is attributed to not only the pre-stored energy in the traps of SAOED but also the self-charging energy through TIEL directly without pre-irradiation.

Since the persistent behavior of SP-PTM lasts ten seconds, it can be applied to transmit complete information in the absence of a continuous power supply through delayed display and visualization. When a contact object was moved on the surface along a Z-shaped trajectory, the motion trail and contact

position were precisely revealed by a recording camera, as shown in Fig. 5a. Moreover, it was also possible to hand-write a string of letters and map them quantitatively, which confirms the unique recording effect of SP-PTM, as shown in Fig. 5b. Obviously, the luminescent intensity varied considerably along the trajectory because the applied force and writing style varied significantly. Thus, to better illustrate the unique TIEL after-glow behavior of the SP-PTM, user identification was performed. Specifically, in order to improve the accuracy and robustness of authentication and identification, supervised machine learning was adopted to build the user profiles for classification. The working process is illustrated in Fig. 5c. Ten users were asked to write the capital letter ''Z'' 20 times on SP-PTM as input to collect the image data. The data sets were first randomly split into training and testing sets. After binary processing of the images, the Gray Level Co-occurrence Matrix
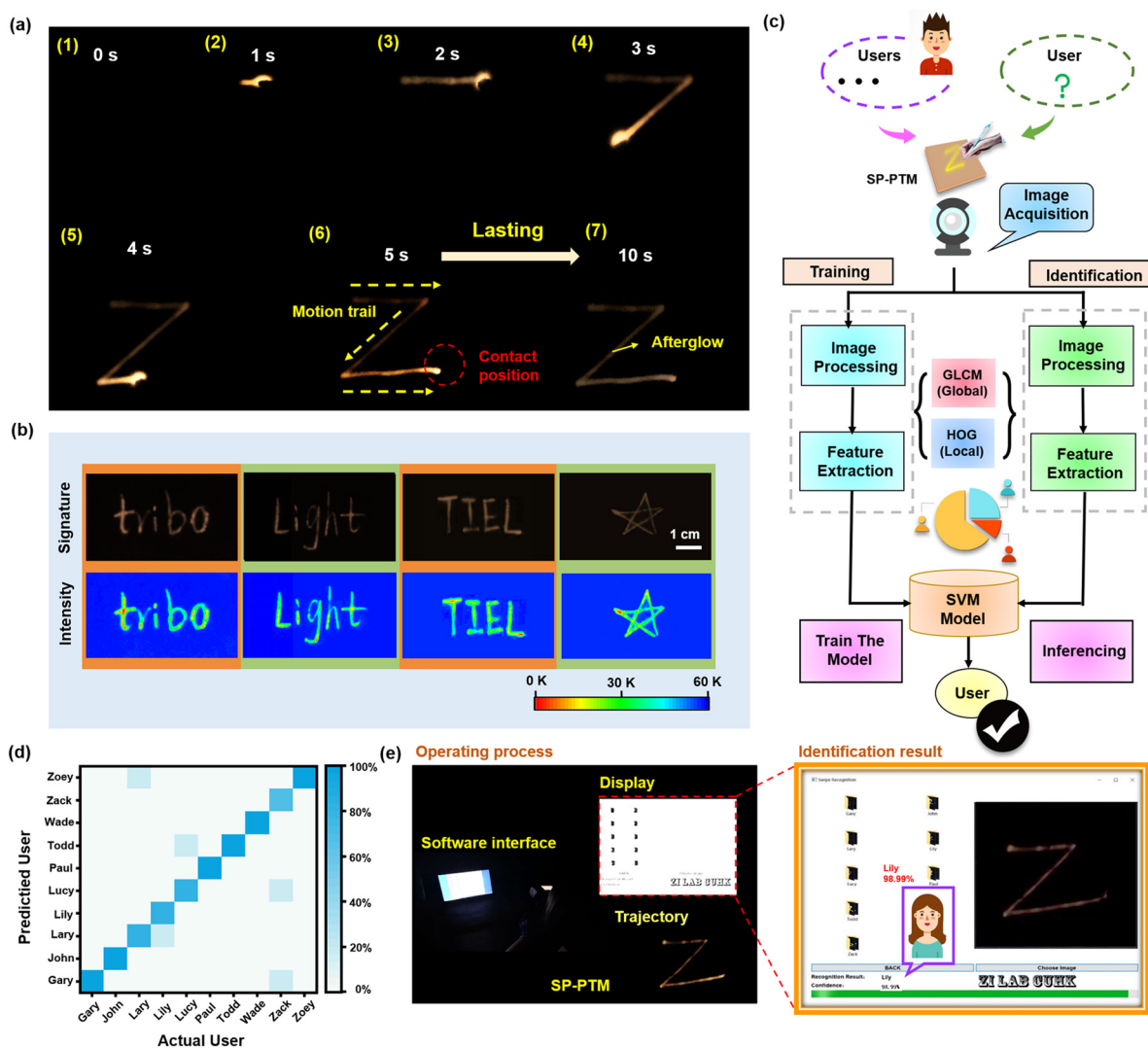

Fig. 5 The application of SP-PTM for wireless user identification. (a) The long-lasting TIEL of SP-PTM before and after the sliding action of the letter ''Z'' on SP-PTM. (b) A continuous trajectory showing a series of words and graphics. Top section: live luminescence images. Bottom section: the corresponding mappings of the luminescence intensity. (c) The process flow of the proposed algorithm for user identification based on the supervised machine learning scheme. (d) The confusion matrices corresponding to the classification results. The numbers in the light-blue boxes indicate the number of misidentified data. (e) The user identification process and the software interface display.

(GLCM) and Histogram of Orientated Gradient (HOG) were adopted to extract the global and local features of the images, respectively. These features were used to train a multi-class Support Vector Machine (SVM) model by the one-versus-the-rest approach. For user identification, the image features were extracted and input into the SVM model, and the inferencing result was obtained by selecting the class with the maximum degree of confidence. Fig. 5d shows the confusion matrices corresponding to the classification results, indicating the effectiveness of the classifier. A detailed description of the classification algorithm can be found in Note S2 (ESI†). Moreover, we built a graphical user interface to interactively demonstrate the user identification process, as presented in Fig. 5e and Movie S3 (ESI†). In this context, the classifier had an overall accuracy of 98.2%.

Furthermore, in addition to the continuous display of the TIEL afterglow in SP-PTM, its versatile responsive properties, including PL, TIEL, and TL effect, were also utilized to produce a responsive multi-mode anti-counterfeiting device (MAD) through a facile screen-printing process, as illustrated in Fig. 6a and the Experimental Section (ESI†). The PDMS-containing distinct phosphors mixtures were sequentially printed onto the template, which was equal-spaced and strip-shaped, thus forming bar codes with customized patterns. An extreme difference in the luminescent bar code was clearly observed when placed under the irradiation of commercial UV light compared with sliding on the surface and thermal-treatment, as shown in Fig. 6b. The optical photograph of the designed bar code under the irradiation of natural light is shown in Fig. 6c. After the MAD was irradiated by a UV light, it exhibited visible patterns with the simultaneous appearance of yellow, green, and orange colors due to the PL effect of the phosphors (Fig. 6d, Mode I). The patterns of the bar code were read out using smartphone scanning software. It was found that the software failed to read any information after a certain period of scanning, as shown in Fig. 6g. Subsequently, when the MAD was stimulated under sliding, it displayed green and orange TIEL emissions continuously owing to its TIEL property under sliding stimuli (Fig. 6e, Mode II). The scanning result of the hidden barcode information was effectively read out as "TI", as shown in Fig. 6h. Finally, the MAD was thermal-treated, and the stored energy was further released to generate an orange TL glow because of its dependence on the traps ((Fig. 6f), Mode III), displaying the read-out information of "EL" (Fig. 6i). The real luminescence and the read-out progress of the as-designed MAD are demonstrated in Movie S4 (ESI†). In addition to addressing the single anti-counterfeiting mode, the proposed MAD can also implant various anti-counterfeiting information through the design of the bar code patterns, which can enhance security, given the current information network anti-counterfeiting technology.
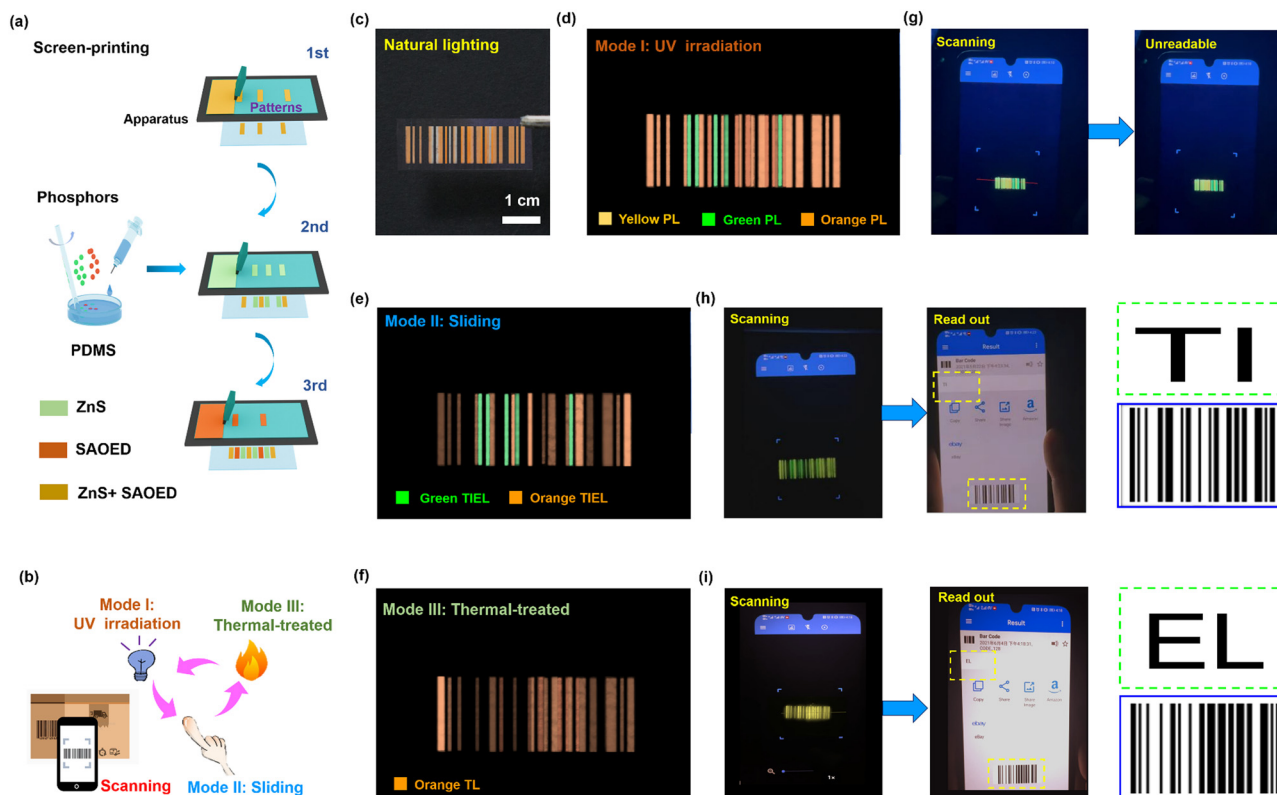
Fig. 6 The application of SP-PTM for multi-mode anti-counterfeiting. (a) The fabrication of the SP-PTM-based bar code pattern. (b) Schematic of the multi-mode SP-PTM-based bar code pattern working under different stimuli. (c) The optical photographs of the barcode pattern produced under natural lighting. Photographs of the bar code pattern under (d) a UV light (365 nm), (e) sliding stimuli, and (f) thermal treatment at 200 °C in the dark. (g, h, and i) The corresponding photographs of the scanning process and information read out using a smartphone.

Materials Horizons

Communication

3. Conclusion

In summary, an all-in-one SP-PTM has been developed with a designed architecture, in which intense and persistent TIEL lasts for about 10 s in the absence of an additional power supply. As confirmed by the theoretical simulations, the improvement of the TIEL intensity is ascribed to the enhancement of electric field variation induced by the polarized ferroelectric ceramic layer. Moreover, the optimal optical performance of the SP-PTM was carefully investigated by controlling several influencing factors. Additionally, the effect of the charge carrier transitions and energy transfer pathways on the optical performance of SP-PTM has been characterized and analysed in depth. Furthermore, the SP-PTM with excellent recording capability and versatile responsive properties is demonstrated in the context of all-optical wireless user identification and multi-mode anti-counterfeiting. Owing to the new methodology for TIEL afterglow with large area and low-cost manufacturing, this novel SP-PTM may remarkably offer opportunities for the development of high-performance mechanical-light energy-conversion systems with recording capability and versatile responsivity, which may have broad potential applications in the fields of mechanical monitoring, human-machine interface, blockchain, *etc.*

Conflicts of interest

There are no conflicts to declare.

Acknowledgements

Notes and references

1 X. D. Wang, H. L. Zhang, R. M. Yu, L. Dong, D. F. Peng, A. H. Zhang, Y. Zhang, H. Liu, C. F. Pan and Z. L. Wang, *Adv. Mater.*, 2015, **27**, 2324–2331.
2 S. M. Jeong, S. Song, K.-I. Joo, J. Kim, S.-H. Hwang, J. Jeong and H. Kim, *Energy Environ. Sci.*, 2014, **7**, 3338–3346.
3 C. Wang, Y. Yan, Y. H. Yuan, C. Y. Ren, Q. Y. Liao, J. Q. Wang, Z. F. Chai, Q. Q. Li and Z. Li, *Matter*, 2020, **2**, 181–193.
4 J. Jang, H. Kim, S. Ji, H. J. Kim, M. S. Kang, T. S. Kim, J. Won, J.-H. Lee, J. Cheon, K. Kang, W. B. Im and J.-U. Park, *Nano Lett.*, 2020, **20**, 66–74.
5 C. H. Li, Q. G. He, Y. Wang, Z. J. Wang, Z. J. Wang, R. Annapooranan, M. I. Latz and S. Q. Cai, *Nat. Commun.*, 2022, **13**, 3914.
6 C. F. Wang, R. H. Ma, D. F. Peng, X. H. Liu, J. Li, B. Jin, A. X. Shan, Y. Fu, L. Dong, W. C. Gao, Z. L. Wang and C. F. Pan, *InfoMat*, 2021, **3**, 1272–1284.
7 X. Qin, Z. R. Cai, M. Su, F. Y. Li, W. Fang, Y. D. Li, X. Zhou, Q. Y. Li, X. Q. Feng, W. B. Li, X. T. Hu, X. D. Wang, C. F. Pan and Y. L. Song, *Adv. Mater.*, 2018, **30**, 1800291.
8 X. Y. Wei, X. D. Wang, S. Y. Kuang, L. Su, H. Y. Li, Y. Wang, C. F. Pan, Z. L. Wang and G. Zhu, *Adv. Mater.*, 2016, **28**, 6656.
9 X. Zhao, Z. Zhang, Q. L. Liao, X. C. Xun, F. F. Gao, L. X. Xu, Z. Kang and Y. Zhang, *Sci. Adv.*, 2020, **6**, 4294.
10 C. Y. Jia, Y. F. Xia, Y. Zhu, M. Wu, S. L. Zhu and X. Wang, *Adv. Funct. Mater.*, 2022, **32**, 2201292.
11 H.-J. Park, S. M. Kim, J. H. Lee, H. T. Kim, W. Seung, Y. Son, T. Y. Kim, U. Khan, N.-M. Park and S.-W. Kim, *ACS Appl. Mater. Interfaces*, 2019, **11**, 5200.
12 J. Y. Li, Z. W. Zhang, X. X. Luo, L. P. Zhu and Z. L. Wang, *ACS Appl. Mater. Interfaces*, 2022, **14**, 4775–4782.
13 X. J. Zhao, S. Y. Kuang, Z. L. Wang and G. Zhu, *Nano Energy*, 2020, **75**, 104823.
14 Z. Tian, L. Su, H. Y. Wang, H. Q. Wang and Y. L. Zi, *Adv. Opt. Mater.*, 2022, **10**, 2102091.
15 L. Su, Q. Xiong, Y. Y. Zhu and Y. L. Zi, *Adv. Funct. Mater.*, 2022, **32**, 2207096.
16 H. L. Wang, L. Su, H. Y. Li, Z. L. Wang and G. Zhu, *Mater. Horiz.*, 2020, **7**, 1144.
17 Y. Wang, H. L. Wang, H. Y. Li, X. Y. Wei, Z. L. Wang and G. Zhu, *ACS Appl. Mater. Interfaces*, 2019, **11**, 13796.
18 L. Su, Q. Xiong, H. Y. Wang and Y. L. Zi, *Adv. Sci.*, 2022, **9**, 2203510.
19 L. Su, Z. Y. Jiang, Z. Tian, H. L. Wang, H. J. Wang and Y. L. Zi, *Nano Energy*, 2021, **79**, 105431.
20 X. D. Wang, M. L. Que, M. X. Chen, X. Han, X. Y. Li, C. F. Pan and Z. L. Wang, *Adv. Mater.*, 2017, **29**, 1605817.
21 B. R. Tian, Z. F. Wang, A. T. Smithd, Y. Q. Baia, J. Z. Lia, N. Zhang, Z. H. Xue and L. Y. Sun, *Nano Energy*, 2021, **83**, 105860.
22 Z. D. Ma, J. Y. Zhou, J. C. Zhang, S. S. Zeng, H. Zhou, A. T. Smith, W. X. Wang, L. Y. Sun and Z. F. Wang, *Mater. Horiz.*, 2019, **6**, 2003–2008.
23 H. J. Wang, X. M. Chen, Z. Tian, Z. Y. Jiang, W. Yu, W. G. Ding and L. Su, *J. Lumin.*, 2020, **228**, 117590.
24 Q. Cheng, Y. Wang, L. Su, H. L. Wang, G. Zhu and W. Yu, *J. Mater. Chem. C*, 2019, **7**, 4567.
25 S. M. Jeong, S. Song, H. Kim, K. Joo and H. Takezoe, *Adv. Funct. Mater.*, 2016, **26**, 4848–4858.
26 Z. Li, H. Zhang and H. Fu, *Opt. Mater.*, 2013, **35**, 451.
27 X. Y. Wei, L. P. Liu, H. L. Wang, S. Y. Kuang, X. X. Zhu, Z. L. Wang, Y. H. Zhang and G. Zhu, *Adv. Mater. Interfaces*, 2017, **5**, 1701063.
28 X. Y. Wei, H. L. Wang, Y. Wang, S. Y. Kuang, X. X. Zhu, J. Z. Zou, L. Wang, X. R. Zeng, F. Rao and G. Zhu, *Nano Energy*, 2019, **61**, 158.

29 D. V. Heggen, R. Zilenaite, E. Ezerskyte, V. Frita, K. Korthout, D. Vandenberghe, J. D. Grave, J. Garrevoet, L. Vincze, D. Poelman, J. J. Joos and P. F. Smet, *Adv. Funct. Mater.*, 2022, **32**, 2109635.

30 N. Zhang, B. R. Tian, Z. F. Wang, A. T. Smith, Z. D. Ma, Z. H. Xue and L. Y. Sun, *Adv. Opt. Mater.*, 2021, **9**, 2100137.

31 Y. X. Shi, R. Lei, F. Y. Li, S. Y. Li, X. L. Tao, P. Yang, X. Y. Chen, Q. Zhao and Z. L. Wang, *ACS Energy Lett.*, 2021, **6**, 3132–3140.

32 Y. Q. Bai, X. P. Guo, B. R. Tian, Y. M. Liang, D. F. Peng and Z. F. Wang, *Adv. Sci.*, 2022, **9**, 2203249.

33 Y. X. Zhang, D. Tu, C. J. Chen, L. Wang, H. W. Zhang, H. Xue, C. H. Yuan, G. R. Chen, C. F. Pan, L. Z. Dai and R.-J. Xie, *Light Sci. Appl.*, 2020, **9**, 182.